Nonlin. Processes Geophys. Discuss., https://doi.org/10.5194/npg-2017-63
Manuscript under review for journal Nonlin. Processes Geophys.
Discussion started: 24 October 2017

Nonlinear Processes in Geophysics
Discussions
Open Access
EGU

Trajectory encounter volume as a diagnostic of mixing potential in fluid flows: connection to diffusivity.

Irina I. Rypina[1], Stefan G. Llewellyn Smith[2], and Larry J. Pratt[1]

[1]Physical Oceanography Department, Woods Hole Oceanographic Institution, 266 Woods Hole Rd., Woods Hole, MA 02543

[2]Department of Mechanical and Aerospace Engineering, Jacobs School of Engineering, UCSD, 9500 Gilman Dr., La Jolla, CA 92093-0411

Corresponding author's email: irypina@whoi.edu

Abstract: Trajectory encounter volume – the volume of fluid that passes close to a reference fluid parcel over some time interval – has been recently introduced as a measure of mixing potential of a flow. Diffusivity is the most commonly used characteristic of turbulent diffusion. We derive the analytical relationship between the encounter volume and diffusivity under the assumption of an isotropic random walk, i.e. diffusive motion, in one and two dimensions. We apply the derived formulas to produce maps of encounter volume and the corresponding diffusivity in the Gulf Stream region of the North Atlantic based on satellite altimetry, and discuss the mixing properties of Gulf Stream rings. Advantages offered by the derived formula for estimating diffusivity from oceanographic data are discussed, as well as applications to other disciplines.

1. Introduction

The frequency of close encounters between different objects or organisms can be a fundamental metric in social and mechanical systems. The chances that a person will meet a new friend or contract a new disease during the course of a day is influenced by the number of distinct individuals that he or she comes into close contact with. The chances that a predator will ingest a poisonous prey, or that a mushroom hunter will mistakenly pick up a poisonous variety, is influenced by the number of distinct species or variety of prey or mushrooms that are encountered. In fluid systems, the exchange of properties such as temperature, salinity or humidity between a given fluid element and its surroundings is influenced by the number of other distinct fluid elements that pass close by over a given time period. In all these cases it is best to think of close encounters as providing the *potential*, if not necessarily the act, of transmission of germs, toxins, heat, salinity, etc.

In cases of property exchange within continuous media such as air or water, it may be most meaningful to talk about a mass or volume passing within some radius of a reference fluid element as this element moves along its trajectory. Rypina and Pratt (2017) introduce a trajectory encounter volume, V, the volume of fluid that comes in contact with the reference fluid parcel over a finite time interval. The increase of V over time is one measure of the mixing potential of

Nonlin. Processes Geophys. Discuss., https://doi.org/10.5194/npg-2017-63
Manuscript under review for journal Nonlin. Processes Geophys.
Discussion started: 24 October 2017

the element, "mixing" being the irreversible exchange of properties between different water parcels. Thus, fluid parcels that have large encounter volumes as they move through the flow field have large mixing potential, i.e., an opportunity to exchange properties with other fluid parcels, and vice versa.

Given the seemingly fundamental importance of close encounters, it is of interest to relate metrics such as V to other bulk measures of interactions within the system. For example, in some cases it may be more feasible to count encounters rather than to measure interactions or property exchanges directly, whereas in other cases the number of encounters might be most pertinent to the process in question, but difficult to measure directly. In many applications, including ocean turbulence, most commonly used metric of mixing is the eddy diffusivity, κ, a quantity that relates transport of fluid elements by turbulent eddies to diffusion, by analogy with molecular diffusion processes. κ can be measured by a variety of means, including dye release (Ledwell et al., 2000; Sundermeyer and Ledwell, 2001; Rypina et al., 2016), surface drifter dispersion (Okubo, 1971; Davis, 1991; LaCasce, 2008, La Casce et al., 2014; Rypina et al. 2012; 2016), and property budgets (Munk, 1966). The purpose of this work is to develop a relationship between V and κ in one and two dimensions. The relationship is not as straightforward as one might first imagine, but can nevertheless be written down straightforwardly in the long-time limit. This is opportune, since the concept of eddy diffusivity is most relevant in the long-time limit.

1.1. Encounter volume as a measure of mixing potential of a flow

For a formal definition of the encounter volume, V, we subdivide the entire fluid into infinitesimal fluid elements with volumes dV_i, and define the encounter volume for each fluid element to be the total volume of fluid that passes within a radius R of it over a finite time interval $t_0 < t < t_0 + T$, i.e.,

$$V(\vec{x}_0; t_0, T, R) = \lim_{dV_i \to 0} \Sigma_i \, dV_i. \quad (1)$$

In practice, for dense uniform grids of trajectories, both the limit and the subscript in the above definition can be dropped, and the encounter volume can be approximated by

$$V \approx N \, \delta V, \quad (2)$$

where the *encounter number*,

$$N(\vec{x}_0; t_0, T, R) = \sum_{k=1}^{K} \mathrm{I}(\min(|\overrightarrow{x_k}(\vec{x}_{0k}; t_0, T) - \vec{x}(\vec{x}_0; t_0, T)|) \leq R), \quad (3)$$

is the number of trajectories that come within a radius R of the reference trajectory over a time $t_0 < t < t_0 + T$. Here the indicator function I is 1 if true and 0 if false, and K is the total number of particles.

Nonlin. Processes Geophys. Discuss., https://doi.org/10.5194/npg-2017-63
Manuscript under review for journal Nonlin. Processes Geophys.
Discussion started: 24 October 2017

As in Rypina and Pratt (2017), we define encounter volume based on the number of encounters with different trajectories, not the total number of encounter events. The encounter volume depends on the starting time, integration time, the number of trajectories, and the encounter radius. The dependences on the first three parameters are typical for all Lagrangian methods (such as, for example, Lagrangian descriptors, complexity measures, FTLE, FSLE, transfer operators, LAVD and others; e.g. Mendoza et al., 2014; Rypina et al., 2012; Shadden et al., 2005; d'Ovidio et al. 2004; Froyland et al., 2007; Haller, 2016. The integration time should be long enough for trajectories to sample the features of interest well, but short enough compared to their lifetime. The grid spacing should be small compared to the sizes of the features of interest, and the encounter radius should to be smaller than about half of the size of the smallest features of interest.

1.2. Diffusive parameterizations of small scales and diffusivity

The combined effects of eddies on redistributing tracers are often represented by an eddy diffusivity (LaCasce, 2008; Vallis, 2006; Rypina et al., 2015; Kamenkovich et al., 2015). The underlying assumption is that the eddy field drives the downgradient tracer transfer, similar to molecular diffusion but with a different (larger) diffusion coefficient. This diffusive parameterization of eddies has been implemented in many non-eddy-resolving oceanic numerical models. The diffusivity is either estimated from data (as, for example, in Okubo, 1971) and often assumed constant in both time and space, or related in some simplified manner to the large-scale flow properties (Visbeck, 1997).

Because the purpose of the diffusivity coefficient is to quantify the intensity of the eddy-induced tracer transfer, i.e., the intensity of mixing, it is tempting to relate it to the encounter volume, which quantifies the mixing potential of a flow and thus is closely related to tracer mixing. Such an analytical connection between the encounter volume and diffusivity could potentially also be useful for the parameterizations of eddy effects in numerical models.

2. Connection between encounter volume and diffusivity

The problem has been framed in mathematical terms in Rypina and Pratt (2017), who outlined some initial steps towards deriving the analytical connection between encounter volume and diffusivity but did not finish the derivation. In this section, we complete the derivation.

2.1. Main idea for the derivation

We seek an analytical expression for the encounter volume, V, and the encounter number, N, i.e., the number of particles that pass within radius R from a reference particle over time, as a function of κ. Let us start by considering the simplest diffusive random walk process in one or two dimensions, where particles take steps of fixed length L in random directions along the x-axis in 1D or along both x- and y-axes in 2D, respectively, at fixed time intervals Δt.

105 The single particle dispersion, i.e., the ensemble-averaged square displacement from the
106 particle's initial position, is $D_{1D} =< (x - x_0)^2 >$ and $D_{2D} =< (x - x_0)^2 + (y - y_0)^2 >$ in 1D
107 or 2D, respectively. For a diffusive process, the dispersion grows linearly with time, and the
108 constant proportionality coefficient that is related to diffusivity. Specifically, $D_{1D} = 2\kappa_{1D}t$ with
109 $\kappa_{1D} = L^2/(2\Delta t)$, and $D_{2D} = 4K_{2D}t$ with $\kappa_{2D} = L^2/(4\Delta t)$.

110 It is convenient to consider the motion in a reference frame that is moving with the reference
111 particle. In that reference frame, the reference particle will always stay at the origin, while other
112 particles will still be involved in a random walk motion, but with the diffusivity twice that in the
113 stationary frame, κ^{moving}=$2\kappa^{stationary}$ (Rypina and Pratt, 2017).

114 The problem of finding the encounter number then reduces to counting the number of randomly
115 walking particles (with diffusivity κ^{moving}) that come within radius R of the origin in the
116 moving frame. This is related to a classic problem in statistics – the problem of a random walker
117 reaching an absorbing boundary, usually referred to as "a cliff" (because once a walker reaches
118 the absorbing boundary, it falls off the cliff), over a time interval t.

119 In the next section we will provide formal solutions; here we simply outline the steps to
120 streamline the derivation. We start by deriving the appropriate diffusion equation for the
121 probability density function, $p(\vec{x}, t)$, of random walkers in 1D or 2D:

122 $$\frac{\partial p}{\partial t} = \kappa \nabla^2 p. \quad (4)$$

123 We place a cliff, $\overrightarrow{x_c}$, at the perimeter of the encounter sphere, i.e., at a distance R from the
124 origin, and impose an absorbing boundary condition at a cliff,

125 $$p(\overrightarrow{x_c}, t) = 0, \quad (5a)$$

126 which removes (or "absorbs") particles that have reached the cliff (see Fig. 1 for a schematic
127 diagram). We then consider a random walker that is initially located at a point $\overrightarrow{x_0}$ outside the
128 cliff at $t = 0$, i.e.,

129 $$p(\vec{x}, t = 0) = \delta(\vec{x} - \overrightarrow{x_0}), \quad (5b)$$

130 and we write an analytical solution for the probability density function satisfying Eqs. (4-5),

131 $$G(\vec{x}, t; \overrightarrow{x_0}, \overrightarrow{x_c}), \quad (6)$$

132 that quantifies the probability to find a random walker initially located at $\overrightarrow{x_0}$ at any location $\vec{x}$
133 outside of the cliff at a later time $t > 0$. In mathematical terms, G is the Green's function of the
134 diffusion equation.

Nonlin. Processes Geophys. Discuss., https://doi.org/10.5194/npg-2017-63
Manuscript under review for journal Nonlin. Processes Geophys.
Discussion started: 24 October 2017

The survival probability, which quantifies the probability that a random walker initially located at $\overrightarrow{x_0}$ at $t = 0$ has "survived" over time t without falling off the cliff, is

$$S(t;\overrightarrow{x_0},\overrightarrow{x_c}) = \int G(\overrightarrow{x},t;\overrightarrow{x_0},\overrightarrow{x_c})d\overrightarrow{x}, \quad (7)$$

where the integral is taken over all locations outside of the cliff. The encounter, or "non-survival", probability can then be written as the conjugate quantity,

$$P_{en}(t;\overrightarrow{x_0},\overrightarrow{x_c}) = 1 - S(t;\overrightarrow{x_0},\overrightarrow{x_c}), \quad (8)$$

which quantifies the probability that a random walker initially located at $\overrightarrow{x_0}$ at $t = 0$ has reached, or fallen off, the cliff over time t. This allows one to write the encounter volume, i.e., the volume occupied by particles that were initially located outside of the cliff and that have reached the cliff by time t, as

$$V(t;\overrightarrow{x_c}) = \int P_{en}(t;\overrightarrow{x_0},\overrightarrow{x_c})d\overrightarrow{x_0}, \quad (9)$$

where the integral is taken over all initial positions outside of the cliff.

2.2. 1D case

Consider a random walker who is initially located at the origin and who takes, with a probability ½, a fixed step Δx to the right or to the left along the x-axis after each time interval Δt. Then the probability to find a walker at a location $x = n\Delta x$ at after $(m + 1)$ steps is

$$p(n\Delta x,(m+1)\Delta t) = 1/2[p\big((n-1)\Delta x,m\Delta t\big) + p\big((n+1)\Delta x,m\Delta t\big)]. \quad (10)$$

Using a Taylor series expansion in Δx and Δt, we can write down the finite-difference approximation to the above expression as

$$p(x,t) + \Delta t\frac{\partial p}{\partial t} = \frac{1}{2}\left[p(x,t) - \Delta x\frac{\partial p}{\partial x} + \frac{\Delta x^2}{2}\frac{\partial^2 p}{\partial x^2} + p(x,t) + \Delta x\frac{\partial p}{\partial x} + \frac{\Delta x^2}{2}\frac{\partial^2 p}{\partial x^2} + O(\Delta x^4)\right] =$$

$$= p(x,t) + \frac{\Delta x^2}{2}\frac{\partial^2 p}{\partial x^2} + O(\Delta x^4), \quad (11)$$

yielding a diffusion equation

$$\frac{\partial p}{\partial t} = \kappa\frac{\partial^2 p}{\partial x^2} \quad (12)$$

with diffusivity coefficient $\kappa = \frac{\Delta x^2}{2\Delta t}$.

Nonlin. Processes Geophys. Discuss., https://doi.org/10.5194/npg-2017-63
Manuscript under review for journal Nonlin. Processes Geophys.
Discussion started: 24 October 2017

160 A Green's function for the 1D diffusion equation without a cliff is a solution with initial
161 condition $p(x, t = 0; x_0) = \delta(x - x_0)$ in an unbounded domain. It takes the form

162 $$G_{unbounded}(x, t; x_0) = \frac{1}{\sqrt{4\pi\kappa t}} e^{-\frac{(x-x_0)^2}{4\kappa t}}. \quad (13)$$

163 A Green's function with the cliff (see Fig. 1 for a schematic diagram), for a solution to the
164 initial-value problem with $p(x, t = 0; x_0) = \delta(x - x_0)$ in a semi-infinite domain, $x \in [-\infty; x_c]$,
165 with an absorbing boundary condition at a cliff, $p(x = x_c, t; x_0) = 0$, can be constructed by the
166 method of images from two unbounded Green's functions as

167 $$G(x, t; x_0, x_c) = \frac{1}{\sqrt{4\pi\kappa t}} (e^{-\frac{(x-x_0)^2}{4\kappa t}} - e^{-\frac{(x-(2x_c-x_0))^2}{4\kappa t}}). \quad (14)$$

168 It follows from (7-9) that the survival or non-encounter probability is

169 $$S(t; x_0, x_c) := \int_{-\infty}^{x_c} G(x, t; x_0, x_c) dx = Erf[\frac{x_c - x_0}{2\sqrt{\kappa t}}], \quad (15)$$

170 the encounter probability is

171 $$P_{en}(t; x_0, x_c) = 1 - S(t) = 1 - Erf\left(\frac{x_c - x_0}{2\sqrt{\kappa t}}\right), \quad (16)$$

172 and the encounter volume is

173 $$V(t; x_c) = \int_{-\infty}^{x_c} P_{en}(t; x_0, x_c) dx_0 = \int_{-\infty}^{x_c} \left(1 - Erf\left[\frac{x_c - x_0}{2\sqrt{\kappa t}}\right]\right) dx_0 = \frac{2}{\sqrt{\pi}}\sqrt{\kappa t}. \quad (17)$$

174 The above formula accounts for the randomly walking particles that have reached the cliff from
175 the left over time t. By symmetry, if the cliff was located to the right of the origin, the same
176 number of particles would be reaching the cliff from the right, so the total encounter volume is

177 $$V(t; x_c) = \frac{4}{\sqrt{\pi}}\sqrt{\kappa t}. \quad (18)$$

178 Note that formula (18) gives the encounter volume, i.e., the volume of fluid coming within radius
179 R from the origin, in a reference frame moving with the reference particle, so the corresponding
180 diffusivity in the right-hand side of (18) is $\kappa^{moving} = 2\kappa^{stationary}$.

181 2.3. 2D case

182 Consider a random walker in 2D, who is initially located at the origin and who takes, with a
183 probability of $1/4$, a fixed step of length Δx to the right, left, up or down after each time interval
184 Δt. Then the probability to find a walker at a location $x = n\Delta x, y = m\Delta x$ at time $t = (m + 1)\Delta t$
185 is

$$p(n\Delta x, (m + 1)\Delta t) = 1/4[p\big((n - 1)\Delta x, m\Delta y, l\Delta t\big) + p\big((n + 1)\Delta x, m\Delta y, l\Delta t\big) +$$

Nonlin. Processes Geophys. Discuss., https://doi.org/10.5194/npg-2017-63
Manuscript under review for journal Nonlin. Processes Geophys.
Discussion started: 24 October 2017

Nonlinear Processes in Geophysics
Discussions
Open Access
EGU

$$+p(n\Delta x,(m-1)\Delta y,l\Delta t)+p(n\Delta x,(m+1)\Delta y,l\Delta t)]. \quad (19)$$

Using a Taylor series expansion in Δx, Δy and Δt, the finite-difference approximation leads to a diffusion equation

$$\frac{\partial p}{\partial t}=\kappa\left(\frac{\partial^2 p}{\partial x^2}+\frac{\partial^2 p}{\partial y^2}\right) \quad (20)$$

with diffusivity coefficient $\kappa=\frac{\Delta x^2}{4\Delta t}$.

To proceed, we need an analytical expression for the Green's function of Eq. (20) with a cliff at a distance R from the origin, i.e., a solution to the initial-value problem with $p(\overrightarrow{x},t=0;\overrightarrow{x_0})=\delta(\overrightarrow{x}-\overrightarrow{x_0})$ for the above 2D diffusion equation on a semi-infinite plane ($r\geq R, 0<\theta\leq 2\pi$), bounded internally by an absorbing boundary (a cliff) located at $r=R$, so that $p(r=R,\theta,t;\overrightarrow{x_0})=0$ (see Fig. 1(right) for a schematic diagram). Here (r,θ) are polar coordinates.

Carlslaw and Joeger (1939) give the answer as

$$G(r,\theta,t;r_0,\theta_0,R)=u+w=\sum_{n=-\infty}^{\infty}(u_n(r,t;r_0,R)+w_n(r,t;r_0,R))\cos n(\theta-\theta_0) \quad (21)$$

where $r_0(\geq R),\theta_0$ denote the source location, and

$$\{u_n,w_n\}=L^{-1}\left\{\bar{u}_n,\bar{w}_n\right\}=\frac{1}{2\pi i}\lim_{T\to\infty}\int_{\gamma-iT}^{\gamma+iT}e^{st}\left\{\bar{u}_n,\bar{w}_n\right\}ds$$

are the inverse Laplace transforms of

$$\bar{u}_n=\frac{1}{2\pi\kappa}\begin{cases}I_n(qr)K_n(qr_0), R<r<r_0\\ I_n(qr_0)K_n(qr), r>r_0\end{cases}\text{ and }\bar{w}_n=-\frac{I_n(qR)}{K_n(qR)}K_n(qr_0)K_n(qr) \quad (22)$$

with $q=\sqrt{\frac{s}{\kappa}}$.

The survival probability (from Eq. (7)) is

$$S(t;r_0,R)=\int_{R^2}G(\overrightarrow{x},t;\overrightarrow{x_0},R)d^2\overrightarrow{x}=\int_0^{2\pi}\int_R^{\infty}\sum_{n=-\infty}^{\infty}(u_n+v_n)\cos n(\theta-\theta_0)\ r\,dr\,d\theta=$$
$$2\pi\int_R^{\infty}(u_0+v_0)\,rdr. \quad (23)$$

Next, we take the Laplace transform of the survival probability and write it in terms of a Laplace variable s as

$$\overline{S}(s,r_0,R)=\int_0^{\infty}e^{-st}S(t;r_0,R)dt=2\pi\int_R^{\infty}(\overline{u_0}+\overline{w_0})\,rdr=\frac{1}{\kappa}\int_R^{r_0}I_0(qr)K_0(qr_0)\,rdr+$$
$$\frac{1}{\kappa}\int_{r_0}^{\infty}I_0(qr_0)K_0(qr)\,rdr-\frac{1}{\kappa}\int_R^{\infty}\frac{I_0(qR)}{K_0(qR)}K_0(qr)K_0(qr_0)\,rdr. \quad (24)$$

Nonlin. Processes Geophys. Discuss., https://doi.org/10.5194/npg-2017-63
Manuscript under review for journal Nonlin. Processes Geophys.
Discussion started: 24 October 2017

Using $\int rI_0(r)dr = rI_1(r)$ and $\int rK_0(r)dr = -rK_1(r)$, and $\lim_{x\to\infty} xK_1(x) = 0$ we find

$$\overline{S}(s;r_0,R) =$$

$$\frac{1}{\kappa}K_0(qr_0)\left[\frac{r}{q}I_1(qr)\right]\Big|_R^{r'} + \frac{1}{\kappa}I_0(qr_0)\left[-\frac{r}{q}K_1(qr)\right]\Big|_R^{\infty} - \frac{1}{\kappa}\frac{I_0(qr_0)}{K_0(qR)}K_0(qr_0)\left[-\frac{r}{q}K_1(qr)\right]\Big|_R^{\infty} =$$

$$\frac{1}{\kappa}\left\{\frac{r_0}{q}\left(I_1(qr_0)K_0(qr_0) + I_0(qr_0)K_1(qr_0)\right) - \frac{a}{q}\frac{K_0(qr_0)}{K_0(qR)}\left(I_1(qR)K_0(qR) + I_0(qR)K_1(qR)\right)\right\}. \quad (25)$$

But $I_1(x)K_0(x) + I_0(x)K_1(x) = \frac{1}{x}$ so

$$\overline{S}(s;r_0,R) = \frac{1}{\kappa}\left(\frac{1}{q^2} - \frac{1}{q^2}\frac{K_0(qr_0)}{K_0(qR)}\right) = \frac{1}{s}\left(1 - \frac{K_0(qr_0)}{K_0(qR)}\right). \quad (26)$$

From (8), the encounter probability $P_{en}(t;\overrightarrow{x_0},R) = 1 - S(t;\overrightarrow{x_0},R)$, and from (9) the encounter volume is

$$V(t;R) = \int_{R^2} P_{en} d^2\overrightarrow{x_0} = \int_0^{2\pi}\int_R^{\infty} P_{en}\, r_0\, dr_0 = 2\pi\int_R^{\infty}[1 - S(t;r_0,R)]r_0\, dr_0\,. \quad (27)$$

We now take the Laplace transform of the encounter number to get

$$\bar{V}(s;R) = \int_0^{\infty} e^{-st}V(t;R)dt = 2\pi\int_R^{\infty}\left[\frac{1}{s} - \overline{S}(s;R)\right]r_0\, dr_0 = 2\pi\int_R^{\infty}\frac{K_0(qr_0)}{K_0(qR)}\frac{r_0}{s}dr_0 =$$

$$\frac{2\pi}{sK_0(qR)}\left[-\frac{r_0}{q}K_1(qr_0)\right]\Big|_R^{\infty} = \frac{2\pi R}{sq}\frac{K_1(qR)}{K_0(qR)} = \frac{2\pi R}{s^{3/2}\kappa^{-\frac{1}{2}}}\frac{K_1\left(\sqrt{\frac{s}{\kappa}}R\right)}{K_0\left(\sqrt{\frac{s}{\kappa}}R\right)}, \quad (28)$$

where we used $\int_0^{\infty} e^{-st}dt = \frac{1}{s}$, $\int K_0(z)z\, dz = -zK_1(z)$, and $\lim_{z\to\infty} K_1(z)$=0.

The explicit connection between the encounter volume and diffusivity is thus given by the inverse Laplace transform of the above expression (28),

$$V(t;R) = L^{-1}\{\bar{V}(s;R)\}. \quad (29)$$

Although numerically straightforward to evaluate, a non-integral analytic form does not exist for this inverse Laplace transform. To better understand the connection between V and κ and the growth of V with time, we next look at the asymptotic limits of small and large time. The small-t limit is transparent, while the long-t limit is more involved.

(a) small-t asymptotics

In the small-t limit, the corresponding Laplace coordinate s is large, giving

$$\bar{V}(s;R) \sim 2\pi R\kappa^{\frac{1}{2}}\frac{1}{s^{3/2}} \quad (30)$$

Nonlin. Processes Geophys. Discuss., https://doi.org/10.5194/npg-2017-63
Manuscript under review for journal Nonlin. Processes Geophys.
Discussion started: 24 October 2017

because $lim_{z\to\infty}\frac{K_1(z)}{K_0(z)}=1$. Noting that $L^{-1}\left\{s^{-\frac{3}{2}}\right\}=\frac{2\sqrt{t}}{\sqrt{\pi}}$, the inverse Laplace transform of the above gives the following simple expression connecting the encounter number and diffusivity at short times:

$$V(t;R)\overset{t\to 0}{\longrightarrow}4R\sqrt{\pi}\,\sqrt{\kappa t}. \tag{31}$$

(b) large-t asymptotics

In the large-t limit, the Laplace coordinate s is small and the asymptotic expansions K_0, K_1 take the form

$$lim_{z\to 0}K_0(z)=-\gamma-\ln\left(\frac{z}{2}\right)+O(\left(\frac{z}{2}\right)^2\ln(\frac{z}{2})), \tag{32}$$

$$lim_{z\to 0}K_1(z)=\frac{1}{z}+\frac{z}{2}[\ln\left(\frac{z}{2}\right)+\gamma-\frac{1}{2}]+O\,(\mathrm{z}^3\ln z), \tag{33}$$

giving

$$\lim_{s\to 0}\bar{V}(s;R)=-\frac{4\pi\kappa}{s^2\ln(\tau s)}-\frac{\pi R^2}{s}+O\left(\frac{1}{s\ln(\tau s)}\right), \tag{34}$$

where

$$\tau=\frac{R^2e^{2\gamma}}{4\kappa}. \tag{35}$$

We now need to take an inverse Laplace transform of $\bar{V}$. The second term in the right-hand side gives $L^{-1}\left\{\frac{\pi R^2}{s}\right\}=\pi R^2$. Llewelyn Smith (2000) discusses the literature for inverse Laplace transforms of the form $(s^\alpha\ln s)^{-1}$ for small s. For our problem, the discussion in Olver (1974, Chap. 8, §11.4) is the most helpful approach. His result (11.13), discarding the exponential term which is not needed here, shows that the inverse Laplace transform of $(s^2\ln s)^{-1}$ has the asymptotic expansion

$$L^{-1}\left\{\frac{1}{s^2\ln s}\right\}\overset{t\to\infty}{\longrightarrow}-t\left(\frac{1}{\ln t}+\frac{1-\gamma}{(\ln t)^2}+O((\ln t)^{-3})\right). \tag{36}$$

Using $L^{-1}\{F(\tau s)\}=\frac{1}{\tau}f(t/\tau)$, we thus obtain the desired connection between the encounter number and diffusivity at long times:

$$V(t;R)\overset{t\to\infty}{\longrightarrow}4\pi\kappa t\left(\frac{1}{\ln\frac{t}{\tau}}+\frac{1-\gamma}{(\ln\frac{t}{\tau})^2}\right)-\pi R^2+O\left(\frac{t}{(\ln\frac{t}{\tau})^3}\right)+O\left(\frac{1}{\ln\frac{t}{\tau}}\right). \tag{37}$$

257 Physically, the time scale τ (Eq. (35)) defines the time at which the dispersion of random
258 particles, $D = 4\kappa\tau$, is comparable to the volume of the encounter sphere, ie., $R^2 e^{2\gamma} \cong \pi R^2$ in
259 2D. Thus for $t \gg \tau$, particles are coming to the encounter sphere "from far away."

260 For practical applications, it is sufficient to only keep the leading order term of the expansion,
261 yielding a simpler connection between encounter number and diffusivity,

262 $$V(t;R) \xrightarrow{t\to\infty} \frac{4\pi\kappa t}{\ln\frac{t}{\tau}} + O\left(\frac{t}{(\ln\frac{t}{\tau})^2}\right). \quad (38)$$

263 Note again that the diffusivity in the right-hand side of Eqs. (28-29), (31) and (38) is
264 $\kappa^{moving}=2\kappa^{stationary}$.

265 2.4. Numerical tests of the derived formulas in 1d and 2d

266 Before applying our results to the realistic oceanic flow, we numerically tested the accuracy of
267 the derived formulas in idealized settings by numerically simulating a random walk motion in 1D
268 and 2D, as described in the beginning of subsections 2.1 and 2.2, respectively. We then
269 computed the encounter number and encounter volume using definition (2-3), and compared the
270 result with the derived exact formulas (18) and (28-29) and with the asymptotic formulas (31)
271 and (38). Note that although formulas (28-29) are exact, the inverse Laplace transform still needs
272 to be evaluated numerically and thus is subject to numerical accuracy, round-off errors etc.; these
273 numerical errors are, however, small, and we will refer to numerical solutions of (28-29) as
274 "exact," as opposed to the asymptotic solutions (31) and (38).

275 The comparison between numerical simulations and theory is shown in Fig. 2. Because the
276 numerically simulated random walk deviates significantly from the diffusive regime over short
277 (< O(100Δt)) time scales, the agreement between numerical simulation and theory is poor at
278 those times in both 1D and 2D. Once the random walkers have executed > 100 time steps,
279 however, the dispersion reaches the diffusive regime, and the agreement between the theory (red)
280 and numerical simulation (black) rapidly improves for both 1D and 2D cases, with the two
281 curves approaching each other at long times. In 2D, the long-time asymptotic formula (38) works
282 well at long times, $t \gg \tau$, as expected. The 2D short-time asymptotic formula (green) agrees well
283 with the exact formula (red) at short times but not with the numerical simulations (black) for the
284 same reason as discussed above, i.e., because the numerically simulated random walk has not yet
285 reached the diffusive regime at those times.

286 3. Application to the altimetric velocities in the Gulf Stream region

287 Sea surface height measurements made from altimetric satellites provide nearly global estimates
288 of geostrophic currents throughout the World Oceans. These velocity fields, previously
289 distributed by AVISO, are now available from the Copernicus Marine and Environment
290 Monitoring Service (CMEMS) website (http://marine.copernicus.eu/), both along satellite tracks

and as a gridded mapped product in both near-real and delayed time. Here we use the delayed-time gridded maps of absolute geostrophic velocities with ¼ deg spatial resolution and temporal step of 1 day, and focus our attention on the Gulf Stream extension region of the North Atlantic Ocean. There, the Gulf Stream separates from the coast and starts to meander, shedding cold- and warm-core Gulf Stream rings from its southern and northern flanks. These rings are among the strongest mesoscale eddies in the ocean. However, their coherence, interaction with each other and with other flow features, and their contribution to transport, stirring and mixing are still not completely understood (Bower et al., 1985; Cherian and Brink, 2016).

Maps showing the encounter volume for fluid parcel trajectories in the region, and the corresponding diffusivity estimates (Fig. 3) could be useful both for understanding and interpreting the transport properties of the flow, as well as for benchmarking and parameterization of eddy effects in numerical models. In our numerical simulations, trajectories were released on a regular grid with $dx = dy \cong 0.07$ deg on 11 Jan 2015 and were integrated forward in time for 90 days using a fifth-order variable-step Runge-Kutta integration scheme with bi-linear interpolation between grid points in space and time. The encounter radius was chosen to be $R = 0.3$ deg in both zonal and meridional directions, i.e., about a third of a radius of a typical Gulf Stream ring. Similar parameter values were used in Rypina and Pratt (2017), although our new simulation was carried out using more recent 2015 velocities instead of 1997 as in that paper.

The encounter volume field, shown in the top left panel of Fig. 3, highlights the overall complexity of the flow and identifies a variety of features with different mixing potential, most notably, several Gulf Stream rings with spatially small low-V (blue) cores and larger high-V (red) peripheries. Although the azimuthal velocities and vorticity – to – strain ratio are large within the rings, the coherent core regions with inhibited mixing potential are small, suggesting that the *coherent* transport by these rings might be smaller than anticipated from the Eulerian diagnostics such as Okubo-Weiss or closed-streamline criteria (Chelton et al., 2011; Abernathey and Haller, 2017). On the other hand, ring peripheries, where the mixing potential is elevated compared to the surrounding fluid, cover larger geographical area than the cores. Thus, while rings inhibit mixing within their small cores, the enhanced mixing on the periphery might be their dominant effect. This is consistent with the results from Rypina and Pratt (2017), but a more thorough analysis is needed to test this hypothesis. Notably, the encounter number is also large along the northern and southern flank of the Gulf Stream jet, with two separate red curves running parallel to each other and a valley in between (although the curves could not be traced continuously throughout the entire region). This enhanced mixing on both flanks of the Gulf Stream Extension current is reminiscent of chaotic advection driven by the tangled stable and unstable manifolds at the sides of the jet (del-Castillo-Negrete and Morrison, 1993; Rogerson et al., 1999; Rypina et al., 2007; Rypina and Pratt, 2017), and is also consistent with the existence of critical layers (Kuo, 1949; Ngan and Sheppard, 1997).

Nonlin. Processes Geophys. Discuss., https://doi.org/10.5194/npg-2017-63
Manuscript under review for journal Nonlin. Processes Geophys.
Discussion started: 24 October 2017

We now apply the asymptotic formula (38) to convert the encounter volume to diffusivity. Because equation (38) is not invertible analytically, we converted V to κ numerically using a look-up table approach. More specifically, we computed V for a wide range of κ's spanning all possible oceanographic values from 0 to $10^9\ cm^2/s$ and we used the resulting table to assign the corresponding κ values to V values in the left panel of Fig. 3. Note that, instead of the long-time asymptotic formula (38) (as in our simulations), it is also possible to use the exact formulas (28-29) to convert V to κ via a table look-up approach. However, because the exact formulas were also derived under the assumption of a diffusive random walk, neither exact nor asymptotic formulas would work well in regions with a non-diffusive behavior. The asymptotic formula has the advantage of being simpler and it also provides for a numerical estimate of the "long-time-limit" time scale, τ (see discussion below).

The diffusivity map that results from converting V to κ using (38) is shown in the top middle panel of Fig. 3. As expected, it has the same spatial variability as the V-map, with large κ at the peripheries of the Gulf Stream rings and at the flanks of the Gulf Stream and small κ at the cores of the rings, near the Gulf Stream centerline and far away from the Gulf Stream current, where the flow is generally slower. The diffusivity values range from $O(10^5)\ cm^2/s$ to $O(10^7)\ cm^2/s$. Using the 1971 Okubo's diffusivity diagram and scaling law, $\kappa_{Okubo}[cm\hat{}2/s] = 0.0103\ l[cm]^{1.15}$, our diffusivity values correspond to spatial scales from $10\ km$ to $650\ km$, thus spanning the entire mesoscale range. This is not surprising considering the Lagrangian nature of our analysis, where trajectories inside the small ($< 50\ km$) low-diffusion eddy cores stay within the cores for the entire integration duration (90 days), whereas trajectories in the high-diffusivity regions near the ring peripheries and at the flanks of the Gulf Stream jet cover large distances, sometimes $> 650\ km$, over 90 days.

The quality, or skill, of the fit (38) varies greatly throughout the domain, with good/poor fit in high-/low-V areas. This is because in the low-V areas, the behavior of fluid parcels is non-diffusive, so the asymptotic diffusive formula (38) works poorly. This is illustrated in the top right panel of Fig. 3, which shows the corresponding scales, τ (from Eq. (35)), throughout the domain. As suggested by our 2D random walk simulations, the long-time asymptotic diffusive formula works well when $t \gg \tau$, but in reality τ values are < 30 days (1/3 of our integration time) only in the highest-V regions, and are ≅ 90 days within the cores of the Gulf Stream rings. This is further illustrated in the lower panel of Fig. 3, which shows the comparison between numerical $V(t)$ (solid) and the fit (38) (dashed) for 3 reference trajectories (with large, intermediate and small τ) that are initially located in the core, periphery and outside of a Gulf Stream ring (blue, magenta, and green, respectively). Clearly, the long-time diffusive approximation (38) is good/bad/completely fails for the red, black and blue curves, respectively, consistent with the values of τ being small/intermediate/large for the 3 trajectories considered. Thus, τ can be used to provide an important additional information about the time scales of

369 particle spreading, and to identify regions with non-diffusive behavior, such as the Lagrangian
370 eddy cores where τ is longer than the trajectory integration time ($\tau > t$).
371
372 In the top panels of Fig. 3 we used the full velocity field to advect trajectories, so both the mean
373 and the eddies contributed to the resulting encounter volumes and the corresponding
374 diffusivities. But what is the contribution of the eddy field alone to this process? To answer this
375 question, we have performed an additional simulation in the spirit of Rypina et al. (2012), where
376 we advected trajectories using the altimetric time-mean velocity field, and then subtracted the
377 resulting encounter volume, V_{mean}, from the full encounter number, V. The result characterizes
378 the contribution of eddies, although strictly speaking $V_{eddy} \neq V - V_{mean}$ because of non-
379 linearity. Note also that because we are interested in the Lagrangian-averaged effects of eddies
380 following fluid parcels, V_{eddy} cannot be estimated by simply advecting particles by the local
381 eddy field alone (see an extended discussion of this effect in Rypina et al., 2012). Not
382 surprisingly, the eddy-induced encounter volumes (lower left panel of Fig. 3) are smaller than the
383 full encounter numbers, with the largest decrease near the Gulf Stream current, where both the
384 mean velocity and the mean shear are large. In other geographical areas, specifically at the
385 peripheries of the Gulf Stream rings, the decrease in V is less significant, so the resulting map
386 retains its overall qualitative spatial structure. The same is true for the diffusivities in the bottom
387 middle panel of Fig. 3. The overall spatial structure of the eddy diffusivity is preserved and
388 matches that in the top panel, but the values decrease, with the largest differences near the Gulf
389 Stream, where some diffusivity values are now $O(10^6)\ cm^2/s$ instead of $O(10^7)\ cm^2/s$. In
390 contrast, κ only decreases, on average, by a factor of 2–3 (instead of an order of magnitude) near
391 the peripheries of the Gulf Stream rings. The long-time diffusive time scale τ generally
392 increases, and the ratio t/τ generally decreases throughout the domain, but the long-time
393 asymptotic formula (38) still works well in high-V regions, specifically on the peripheries of the
394 Gulf Stream rings where τ is still significantly less than t.
395
396 4. Discussion and Summary

397 With many new diagnostics being developed for characterizing mixing in fluid flows, it is
398 important to connect them to the well-established conventional techniques. This paper is
399 concerned with understanding the connection between the encounter volume, which quantifies
400 the mixing potential of the flow, and diffusivity, which quantifies the intensity of the down-
401 gradient transfer of properties. Intuitively, both quantities characterize mixing and it is natural to
402 expect a relationship between them, at least in some limiting sense. Here, we derived this
403 anticipated connection for a diffusive process, and we showed how this connection can be used
404 to produce maps of spatially-varying diffusivity, and to gain new insights into the mixing
405 properties of eddies and the particle spreading regime in realistic oceanic flows.

406 When applied to the altimetry-based velocities in the Gulf Stream region, the encounter volume
407 and diffusivity maps show a number of interesting physical phenomena related to transport and

mixing. Of particular interest are the transport properties of the Gulf Stream rings. The materially-coherent Lagrangian cores of these rings, characterized by very small diffusivity, are smaller than expected from earlier Eulerian diagnostics (Chelton et al., 2011). The periphery regions with enhanced diffusivity are, on the other hand, large, raising a question about whether the rings, on average, act to preserve coherent blobs of water properties or to speed up the mixing. The encounter volume, through the derived connection to diffusivity, might provide a way to address this question and to quantify the two effects, clarifying the role of eddies in transport and mixing.

Reliable data-based estimates of eddy diffusivity are needed for parameterizations in numerical models. The conventional estimation of diffusivity from Lagrangian trajectories via calculating particle dispersion requires large numbers of drifters or floats (LaCasce, 2008). It would be useful to have a technique that would work with fewer instruments. The derived connection between encounter volume and diffusivity might help in achieving this goal. Specifically, one could imagine that if an individual drifting buoy was equipped with an instrument that would measure its encounter volume – the volume of fluid that came in contact with the buoy over time t – then the resulting encounter volume could be converted to diffusivity using the derived connection. This would allow estimating diffusivity using a single instrument.

In the field of social encounters, it is becoming possible to construct large data sets by tracking cell phones, smart transit cards (Sun, et al. 2013), and bank notes (Brockmann, et al. 2006). As was the case for the Gulf Stream trajectories, some of the behavior appears to be diffusive and some not so. Where diffusive/random walk behavior is relevant, it may be easier to accumulate data on close encounters rather than on other metrics using, for example, autonomous vehicles and instruments that are able, through local detection capability, to count foreign objects that come within a certain range.

Acknowledgments: This work was supported by the NSF grants OCE-1558806 and EAR-1520825, and NASA grant NNX14AH29G.

References

Abernathey, R. P., and G. Haller (2017). Transport by Coherent Lagrangian Vortices in the Eastern Pacific, submitted

Bower., A. S., H. T. Rossby, and J. L. Lillibridge (1985). The Gulf Stream-Barrier or blender? J. Phys. Oceanogr., 15, 24–32.

Brockmann, D., L. Hufnagel, T. Geisel (2006). The scaling laws of human travel. *Nature* 439(7075):462-465.

Carslaw, H. S.; Jaeger, J. C. (1939). On Green's functions in the theory of heat conduction. Bull. Amer. Math. Soc. 45 (1939), no. 6, 407--413.https://projecteuclid.org/euclid.bams/1183501899

Cherian, D.A. and K.H. Brink (2016). Offshore Transport of Shelf Water by Deep-Ocean Eddies. *J. Phys. Oceanogr.*, 46, 3599–3621, https://doi.org/10.1175/JPO-D-16-0085.1

Chelton, D. B., M. G. Schlax, and R. M Samelson (2011). Global observations of nonlinear mesoscale eddies. *Prog. Oceanogr.*, 91, 167-216

del-Castillo-Negrete, D. and P. J. Morrison (1993). Chaotic transport of Rossby waves in shear flow. Phys. Fluids A, 5 (4), 948-965.

Davis, R. E. (1991). Observing the general circulation with floats. *Deep-Sea Res.*, **38**, 531-571.
d'Ovidio F., Fernandez V., Hernandez-Garcıa E., Lopez C. (2004). Mixing structures in the Mediterranean Sea from finite size Lyapunov exponents. *Geophys. Res. Lett.* 31:L17203

Froyland, G., Padberg, K., England, M. H., and Treguier, A. M. (2007). Detection of coherent oceanic structures via transfer operators, Phys. Rev. Lett., 98, 224503, doi:10.1103/PhysRevLett.98.224503

Haller, G., Hadjighasem, A., Farazmand, M., and Huhn, F. (2016). Defining coherent vortices objectively from the vorticity, J. Fluid Mech., 795, 136–173, doi:10.1017/jfm.2016.151, 2016.

Kamenkovich, I., I. I. Rypina, and P. Berloff (2015). Properties and Origins of the Anisotropic Eddy-Induced Transport in the North Atlantic. *Journal of Physical Oceanography*, **45**, 778-791, doi:10.1175/JPO-D-14-0164.1.

Kuo, H., 1949: Dynamic instability of two-dimensional non-divergent flow in a barotropic atmosphere. *J. Meteor.*, **6,** 105–122

LaCasce, J. H. (2008). Statistics from Lagrangian observations. Prog. Oceanogr., 77, 1-29, doi:10.1016/j.pocean.2008.02.002.

LaCasce, J. H., Ferrari, r., Marshall, J., Tulloch,R., Balwada, D. & Speer, K. (2014). Float-derived isopycnal diffusivities in the DIMES experiment. Journal of Physical Oceanography. ISSN 0022-3670. 44(2), s 764- 780. doi: 10.1175/JPO-D-13-0175.1

Ledwell, J. R., A. J. Watson, and C. S. Law (1998). Mixing of a tracer in the pycnocline, J. Geophys. Res., 103(C10), 21499–21529, doi:10.1029/98JC01738.

Ledwell, J. R., E. T. Montgomery, K. L. Polzin, L. C. St. Laurent, R. W. Schmitt & J. M. Toole, (2000). Evidence for enhanced mixing over rough topography in the abyssal ocean. Nature, 403, 179-182, doi:10.1038/35003164

Llewellyn Smith, S. G. (2000). The asymptotic behaviour of Ramanujan's integral and its application to two-dimensional di_usion-like equations, Euro. Jnl of Applied Mathematics, 11:13-28

Mendoza, C., Mancho, A. M., and Wiggins, S. (2014). Lagrangian descriptors and the assessment of the predictive capacity of oceanic data sets, Nonlin. Processes Geophys., 21, 677–689, doi:10.5194/npg-21-677-2014

Munk, W. H. (1966). *Abyssal Recipes, Deep-Sea Res., 13, 707-730.*

Ngan, K., and T. G. Shepherd, 1997: Chaotic mixing and transport in Rossby wave critical layers. *J. Fluid Mech.,* **334,** 315–351.

Okubo, A. 1971. Ocean diffusion diagram. *Deep-Sea Res.*, **18**, 789-802.

Olver, F. W. J. (1974). Asymptotics and Special Functions. Academic.

Rogerson, A. M., P. D. Miller, L. J. Pratt, and C.K.R.T. Jones (1999). Lagrangian Motion and Fluid Exchange in a Barotropic Meandering Jet. *J. Phys. Oceanogr.* **29**, 2635-2655.

Rypina, I. I., M. G. Brown, F. J. Beron-Vera, H. Kocak, M. J. Olascoaga, and I. A. Udovydchenkov (2007). On the Lagrangian dynamics of atmospheric zonal jets and the permeability of the stratospheric polar vortex. *J. Atmos. Sci.*, **64**, 3595-3610.

Rypina, I. I., A. Kirincich, S. Lentz, M. Sundermeyer (2016). Investigating the eddy diffusivity concept in the coastal ocean. *J. Phys. Oceangr.*, **46**(7), 2201-2218, DOI: http://dx.doi.org/10.1175/JPO-D-16-0020.1

Rypina, I. I., and L. J. Pratt (2017). Trajectory encounter volume as a diagnostic of mixing potential in fluid flows. *Nonlin. Processes Geophys.*, 24, 189-202, https://doi.org/10.5194/npg-24-189-2017

Rypina, I. R., I. Kamenkovich, P. Berloff and L. J. Pratt (2012). Eddy-Induced Particle Dispersion in the Near-Surface North Atlantic. *J. Phys. Ocean.* DOI: 10.1175/JPO-D-11-0191.1

Rypina, I. I., Scott, S. E., Pratt, L. J., and Brown, M. G. (2011). Investigating the connection between complexity of isolated trajectories and Lagrangian coherent structures, Nonlin. Processes Geophys., 18, 977–987, doi:10.5194/npg-18-977-2011

Shadden, S. C., Lekien, F., and Marsden, J. E.(2005). Definition and properties of Lagrangian coherent structures from finite-time Lyapunov exponents in two-dimensional aperidic flows, Physica D, 212, 271–304

Sun, L. K. W. Axhausen, L. Der-Horng and X Huang (2013). Understanding metropolitan patterns of daily encounters. PNAS 110(34), 13774-13779.

Sundermeyer, M., and J. Ledwell (2001). Lateral dispersion over the continental shelf: Analysis of dye release experiments. J. Geophys. Res., 106, 9603–9621, doi:10.1029/2000JC900138.

Vallis, G. K. (2006). Atmospheric and Oceanic Fluid Dynamics. Cambridge University Press, 745 pp.

Visbeck, M., J. Marshall, T. Haine, and M. Spall (1997). Specification of eddy transfer coefficients in coarse-resolution ocean circulation models. J. Phys. Oceanogr., 27, 381–402.

Nonlin. Processes Geophys. Discuss., https://doi.org/10.5194/npg-2017-63
Manuscript under review for journal Nonlin. Processes Geophys.
Discussion started: 24 October 2017

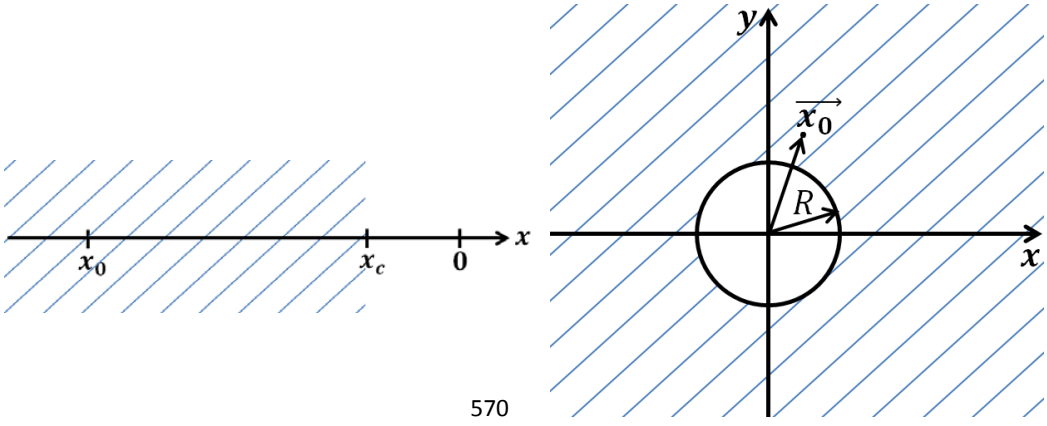

570

571 **Figure 1. Schematic diagram in 1D (left) and 2D (right). Hatched areas show semi-infinite domains outside of the cliff.**

572

573

574

575

576

577

578

579

580

581

Nonlin. Processes Geophys. Discuss., https://doi.org/10.5194/npg-2017-63
Manuscript under review for journal Nonlin. Processes Geophys.
Discussion started: 24 October 2017

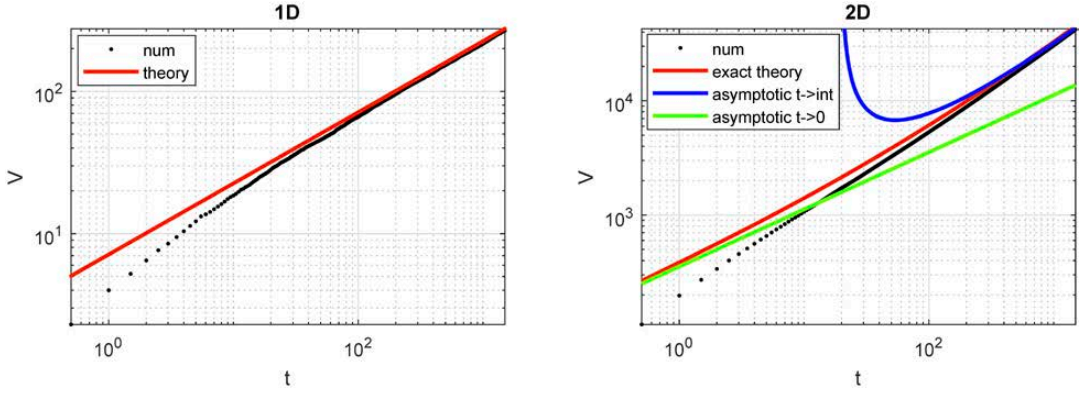

582

583 **Figure 2. Comparison between theoretical expression (red, green, blue) and numerical estimates (black) of the encounter**
584 **volume for a random walk in 1D (left) and 2D (right). In both, $\kappa = 5$ and $\Delta t = 0.5$. In 2D, $\tau \cong 20$.**

585

586

587

588

589

Nonlin. Processes Geophys. Discuss., https://doi.org/10.5194/npg-2017-63
Manuscript under review for journal Nonlin. Processes Geophys.
Discussion started: 24 October 2017

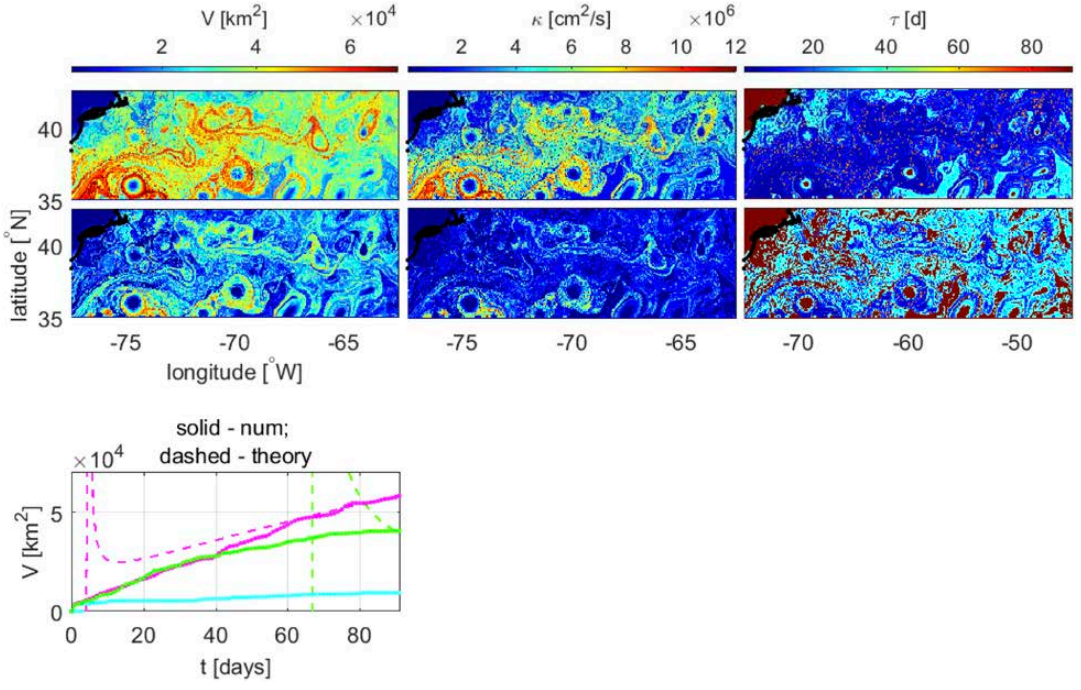

590

591 **Figure 3. Encounter number (left), diffusivity (middle), and diffusive time-scale (right) for the full flow (top) and for the eddy**
592 **component of the flow (bottom). The encounter volume was computed on 11/01/2015 over 90 days with a radius of 3°. The**
593 **lower panel shows comparison between N and its asymptotic fit (38) for the 3 reference trajectories located in the core,**
594 **periphery and outside (blue, magenta, green) of the Gulf Stream ring.**

595